of the two members of the cascade must be identical. This is in agreement with experiment.[1]

In summary, the F^{18} 1.131-MeV level has $J^\pi = 5^+$ and decays by $E2$ emission to the 0.937-MeV level. It has a mean lifetime[1] of 225±8 nsec, which corresponds to an $E2$ strength of 4.62±0.16 Weisskopf units. These properties have recently been discussed by Poletti and Fossan.[1]

ACKNOWLEDGMENTS

I would like to thank A. R. Poletti and D. B. Fossan for a helpful discussion of their work.

PHYSICAL REVIEW VOLUME 163, NUMBER 4 20 NOVEMBER 1967

Determination and Distorted-Wave Born-Approximation Analysis of the Neutron Polarization in the $C^{12}(He^3,n)O^{14}$ Reaction*

L. A. SCHALLER,† R. S. THOMASON,‡ N. R. ROBERSON, AND R. L. WALTER
Duke University, Durham, North Carolina

AND

R. M. DRISKO
Oak Ridge National Laboratory, Oak Ridge, Tennessee

(Received 19 May 1967)

Nine angular distributions of the neutron polarization produced in the $C^{12}(He^3,n)O^{14}$ (ground-state) reaction were determined for He^3 energies from 2.24 to 3.70 MeV. High polarizations were found at all energies, the extreme values being −0.87 at 2.39 MeV and 50°, and +0.72 at 3.70 MeV and 40°. Below 3.2 MeV, the neutron yield at 0° and the differential cross sections exhibit compound-nuclear effects. Above this energy, the 0° yield curve is structureless, and the cross section shows pronounced $l=0$, diproton stripping patterns. Also, the three polarization distributions between 3.30 and 3.70 MeV are similar. An attempt was made to fit the 3.70-MeV (He^3,n) cross section and neutron polarization distributions with a distorted-wave Born-approximation (DWBA) analysis. Prior to this analysis, He^3 elastic-scattering data were obtained over the region from 3.6 to 3.8 MeV, and optical-model parameters for the incident channel were extracted. Considering the possible compound-nuclear effects which were neglected in the fitting procedure, reasonable results were achieved with the DWBA code. One striking result was that the predicted polarization is insensitive to the He^3 spin-orbit strength.

I. INTRODUCTION

RECENTLY, (He^3,n) reactions have been studied with considerable interest, since such reactions lead to levels of proton-rich nuclei which otherwise are difficult to populate. In order to examine the reaction mechanisms involved, polarization measurements, in conjunction with differential cross-section data, are particularly useful. Angular distributions of the outgoing neutron polarization, determined for several incident He^3 energies, help establish the importance of compound nucleus and direct-reaction contributions. If the reaction proceeds via double stripping, the transferred diproton has predominantly an intrinsic spin $S=0$. The same feature applies to a (t,p) double-stripping reaction, where a dineutron is transferred. On the other hand, in (He^3,p) reactions the transfer of a neutron-proton cluster is complicated by the fact that neither $S=0$ nor $S=1$ is strongly preferred. The treatment of (He^3,n) or (t,p) polarization data also has certain theoretical advantages compared to deuteron stripping polarizations, where an incoming particle of spin 1 and the D-state admixture to the deuteron wave function have to be taken into account. Although a large number of (d,n) and (d,p) polarization measurements have been performed,[1,2] no (He^3,n) or (t,p) polarization determinations have been reported to date. In fact, the only reported polarization measurements for two-nucleon transfer reactions are the (He^3,p) proton polarization measurements by Simons *et al.*[3] The scarcity of (He^3,n) and (He^3,p) polarization data is partly due to the low cross section of these reactions and partly due to the emphasis previously given to single-nucleon stripping studies.

The present paper reports the measurement of nine angular distributions of the neutron polarization for the $C^{12}(He^3,n)O^{14}$ [ground state (g.s.)] reaction in the He^3

* Work supported in part by the U. S. Atomic Energy Commission.

† Present address: University of Fribourg, Fribourg, Switzerland.

‡ National Defense Education Act Graduate Fellow.

[1] W. Haeberli, in *Proceedings of the Conference on Direct Interactions and Nuclear Reaction Mechanisms, Padua, 1962*, edited by E. Clementel and C. Villi (Gordan and Breach Science Publishers, Inc., New York, 1963), p. 580.

[2] D. W. Miller, in *Proceedings of the Second International Symposium on Polarization Phenomena of Nucleons* (Birkhäuser Verlag, Basel and Stuttgart, 1966), p. 410.

[3] D. G. Simons and R. Detenbeck, Phys. Rev. **137**, B1471 (1965); D. G. Simons, Bull. Am. Phys. Soc. **11**, 301 (1966).

energy range from 2.24 to 3.70 MeV. Carbon was chosen as a target material since the $C^{12}(He^3,n)O^{14}$ (g.s.) reaction, viewed as a stripping process, can only involve the transfer of a diproton with intrinsic spin $S=0$ and orbital angular momentum $l=0$. Thus spin-dependent distortions in the incident and/or the outgoing channel are solely responsible for polarization effects. In addition, the experimental complications are reduced with carbon as a target since for the energy range investigated, only neutrons which leave O^{14} in the g.s. can be produced. A detailed description of the experimental method and the neutron polarization angular distributions obtained thereby are given in Sec. II.

Excitation functions and/or angular distributions of the differential neutron cross section have been measured by Bromley *et al.*[4] in the energy range below 3 MeV, by Gale *et al.*[5] for energies between 4.1 and 5.7 MeV, by Towle and Macefield[6] from 2.0 to 5.7 MeV, and by Deshpande *et al.*[7] above 5.5 MeV. Recently, Din *et al.*[8] measured excitation functions at 0° and 90° for bombarding energies from 1.8 to 5.2 MeV and eight angular distributions between 2.3 and 5.2 MeV, and Hollandsworth *et al.*[9] measured five angular distributions between 2.4 and 3.8 MeV. For energies above 4 MeV, Newn's plane-wave double-stripping theory[10] has been applied to the angular-distribution data.[5,6] The fits, assuming an $l=0$ diproton transfer, were only partly successful. This fact is not surprising, since, especially at lower He^3 energies, the distorting effects of the nuclear potential on the incident and emergent particles play an important role. A DWBA treatment should provide a more meaningful comparison with experiment and also will predict polarizations generally different from zero. Even though low incident energy and light target nucleus provide an unfavorable combination,[11] a distorted-wave Born-approximation (DWBA) analysis was attempted at 3.7 MeV, the highest energy of the present polarization experiment. In order to obtain optical-model parameters for the entrance channel, $C^{12}(He^3,He^3)$ elastic-scattering angular distributions and excitation functions were measured in the energy range 3.5–3.9 MeV. These measurements are described in Sec. III. Since neutron elastic scattering from the residual O^{14} nucleus is experimentally not feasible, the optical-model parameters for the exit channel were estimated from other elastic-scattering data on light nuclei[12–17] and were varied within reasonable limits in order to obtain a better fit to the $C^{12}(He^3,n)$ neutron angular distributions and polarizations. The procedure is described in more detail in Sec. IV, which deals with the DWBA analysis. Finally, in a discussion section (Sec. V), the results are summarized.

II. POLARIZATION EXPERIMENT

A. Experimental Method

A singly charged He^3 beam[18] from the Duke University 4-MeV Van de Graaff accelerator was incident on a self-supporting carbon foil. The beam intensity was generally between 6 and 8 μA. The accelerator voltage was calibrated by means of the $C^{12}(He^3,n)$ threshold at $E_{He^3}=1.436$ MeV[19] and the $Li(p,n)$ threshold at $E_p=1.881$ MeV. The latter reaction was also employed to obtain the target thickness by inserting the self-supporting carbon foils in front of the Li target and measuring the resultant threshold energy shift. Several carbon targets were used during the course of the experiment. Their thicknesses to the He^3 beam ranged from 160 to 210 keV. The polarization P_1 of the neutrons emitted at angle θ_1 was determined in a manner similar to the one described by Sawers *et al.*,[20] that is, after having passed through a 90° spin-precession solenoid, the neutrons were incident on a He^4-gas scintillator filled with 130 atm of purified helium and 5 atm of xenon. The helium-scattered neutrons were detected at an angle θ_2 by both "up" and "down" plastic detectors of identical dimensions $2.5\times5.1\times10.2$ cm^3. The distance between carbon target and helium scintillator was 1 m, while the center-to-center distance from the helium cell to each of the plastic detectors was 14 cm. The angle θ_2 was chosen to yield a maximum of the product $P_2\sqrt{\sigma}$, where P_2 is the n-He analyzing power and σ is the n-He differential scattering cross section. Thus θ_2 varied from 60° for incident neutrons with an energy of 600 keV to 110° for neutron energies above 1.8 MeV.

Details of the electronics have been described by Meier *et al.*[21] In brief, a linear signal from the helium

[4] D. A. Bromley, E. Almquist, H. E. Gove, A. E. Litherland, A. B. Paul, and A. J. Ferguson, Phys. Rev. **105**, 957 (1957).
[5] N. H. Gale, J. B. Garg, J. M. Calvert, and K. Ramavataram, Nucl. Phys. **20**, 313 (1960).
[6] J. H. Towle and B. E. F. Macefield, Proc. Phys. Soc. (London) **77**, 399 (1961).
[7] V. K. Deshpande, H. W. Fulbright, and J. W. Verba, Nucl. Phys. **52**, 457 (1964).
[8] G. U. Din, H. M. Kuan, and T. W. Bonner, Nucl. Phys. **50**, 267 (1964).
[9] C. E. Hollandsworth (private communication).
[10] H. C. Newns, Proc. Phys. Soc. (London) **76**, 489 (1960).
[11] G. R. Satchler, Nucl. Phys. **85**, 273 (1966).
[12] P. E. Hodgson, *The Optical Model of Elastic Scattering* (Oxford University Press, London, 1963), pp. 73–106.
[13] W. R. Smith and E. V. Ivash, Phys. Rev. **131**, 304 (1963).
[14] D. R. Winner and R. M. Drisko, University of Pittsburgh Technical Report, 1965 (unpublished).
[15] F. G. Perey, in *Proceedings of the Second International Symposium on Polarization Phenomena of Nucleons* (Birkhäuser Verlag, Basel and Stuttgart, 1966), p. 191; L. Rosen, *ibid.*, p. 253; E. E. Gross, R. H. Bassel, L. N. Blumberg, A. Van der Woude, and A. Zucker, *ibid.*, p. 336.
[16] B. A. Robson, Nucl. Phys. **86**, 649 (1966).
[17] D. G. Gerke, D. R. Tilley, N. R. Fletcher, and R. M. Williamson, Nucl. Phys. **75**, 609 (1966).
[18] N. R. Roberson, D. R. Tilley, and H. R. Weller, Nucl. Instr. Methods **33**, 84 (1965).
[19] J. W. Butler and R. O. Bondelid, Phys. Rev. **121**, 1770 (1961).
[20] J. R. Sawers, Jr., F. O. Purser, and R. L. Walter, Phys. Rev. **141**, 825 (1966).
[21] M. M. Meier, L. A. Schaller, and R. L. Walter, Phys. Rev. **150**, 821 (1966).

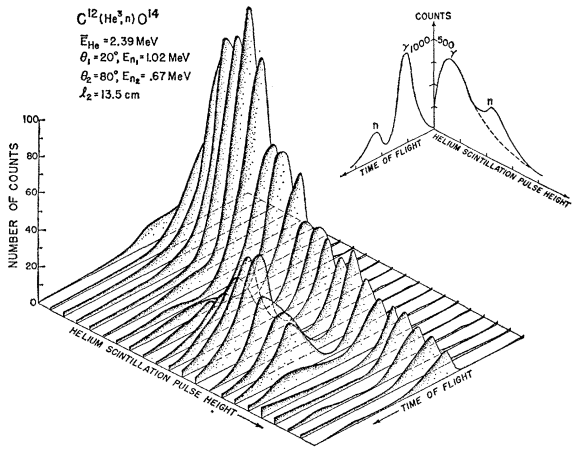

FIG. 1. Isometric display of a typical time-energy spectrum. The small peak is due to neutrons, the large elongated peak is due to γ pulses. The inset shows the sum of counts in the main figure as a function of time of flight and as a function of energy.

scintillator was supplied to a 400 channel analyzer and gated by fast coincidences between the anode pulses from the helium scintillator and from the up detector or the down detector, respectively. The resolving time of the coincidence circuit, $2\tau \sim 10$ nsec, was usually sufficiently short to separate the neutrons from the γ background, but long enough to include all the neutrons. The total energy resolution of the linear signal, composed of the intrinsic helium scintillator resolution, the target thickness, and the geometry employed, amounted to about 20% for 2-MeV neutrons. The over-all time-energy separation is illustrated in a novel way in Fig. 1. Here a two-dimensional spectrum which was recorded using the newly installed "on-line" computer[22] is shown. The time-of-flight spectrum of the "fast" events occurring in the helium scintillator and in the up detector was supplied to the x axis of the computer's multichannel analyzer, the linear helium scintillation spectrum, to the y axis. The energy- and time-integrated counts of the isometric display, projected on the time axis and on the energy axis, respectively, are shown in the inset of Fig. 1. In the inset it can be seen that the γ pulses extend all the way out on the energy axis, but are timewise quite well separated from the neutron pulses. However, at higher neutron energies where the neutron flight time is shorter, the high-energy γ interactions begin to interfere somewhat with the neutron pulses. Nevertheless, this two-parameter analysis indicated that, for most energies and angles, the n-γ separation by means of fast coincidences was sufficient. In order that the data could be processed by computer programs already available, the method outlined at the beginning of this section was employed in the polarization runs (see also Ref. 21).

[22] N. R. Roberson, D. R. Tilley, and M. B. Lewis, Bull. Am. Phys. Soc. **10**, 55 (1965).

B. Measurements and Results

Neutron-polarization distributions were taken in energy steps of approximately 200 keV from 2.24- to 3.70-MeV He^3 energy for reaction angles θ_1 from 10° to 140°. The statistical accuracy of the asymmetry values ϵ was generally between ± 0.03 and ± 0.06, corresponding to running times of 1–2 h per angle. The values P_2, based on the Dodder-Gammel phase shifts[23] and averaged over the given geometry, ranged from 0.63 to 0.90.

Background due to accidental coincidences was generally less than 5%. Background not originating directly from target radiation was determined by inserting a composite paraffin and lead plug in the solenoid core and measuring gated helium recoil spectra. Only a few measurements at selected energies and angles were taken. Because of this room background, the asymmetries ϵ typically had to be increased in magnitude by about 7% of their values. Still, on the average, a nonsubtractable background persisted through most of the measurements. Its magnitude generally fluctuates from 0 to 10%, increasing to about 25% at a few backward angles with very low neutron-production cross sections. It amounts to about 15% for reaction angles $\theta_1 = 10°$ and $\theta_1 = 20°$ at incident He^3 energies above 3 MeV. This nonsubtractable background is believed to be associated with pulses from γ rays which overlap the neutron-coincidence peak. γ rays originate in the C^{12} target from a variety of $C^{12}+He^3$ reactions, especially from the decay of various excited states in N^{14}, and from the annihilation radiation of the β^+ active residual nuclei O^{14} and C^{11} (Ref. 24). In the data analysis, the reasonable assumption was made that the

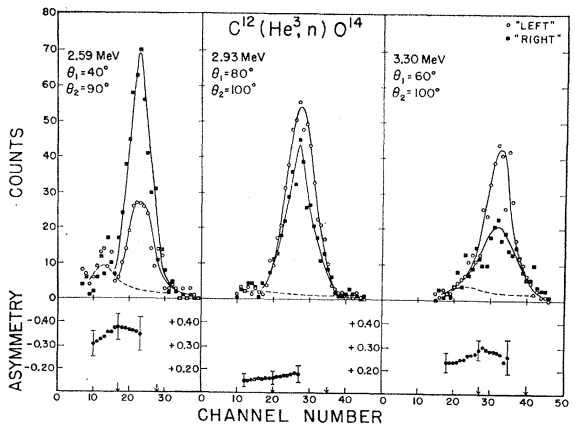

FIG. 2. Three samples of gated-helium recoil spectra. The solid lines are smooth lines drawn through the data points. The dashed lines indicate nonaccidental background as discussed in the text. The lower portion of the figure shows the asymmetry as a function of lower bias channel.

[23] D. C. Dodder and J. L. Gammel, Phys. Rev. **88**, 520 (1952).
[24] T. Lauritsen and F. Ajzenberg-Selove, in *Nuclear Data Sheets*, compiled by K. Way *et al.* (Printing and Publishing Office, National Academy of Sciences–National Research Council, Washington 25, D. C.), NRC 61-5,6-197 and 61-5,6-119.

nonsubtractable background as well as accidental and room backgrounds are unpolarized.

In order to minimize the effect of room background and nonsubtractable background, the peak region of the gated He-recoil spectrum was restricted in a manner similar to the one described by Andress *et al.*,[25] and by Meier *et al.*,[21] that is, the asymmetry was calculated as a function of a lower cutoff channel. The upper limit was kept constant and was chosen at the channel above the peak where the counts dropped below $\frac{1}{5}$ of the peak height. The lower portion of Fig. 2 shows three typical plots of the asymmetry as a function of lower cutoff channel. The error bars represent the statistical standard deviation based on the foreground and background counts. The range of channels included in the asymmetry calculation for the polarization distributions is indicated by arrows. The upper part of Fig. 2 shows the gated He-recoil spectra from which the asymmetries were obtained. The open circles refer to the sum (called "left") of counts in the up detector with positive current flowing through the solenoid and in the down detector with negative solenoid current. The black squares represent the sum (called "right") of counts in the up detector with negative solenoid current and in the down detector with positive solenoid current, respectively. Accidental coincidences have been subtracted. The dashed lines underneath the peaks indicate the sum of the measured room background and the nonsubtractable background. This latter background was extracted for each energy and angle by adding the left and the right counts in each channel and comparing the shape of the resulting peak with a Gaussian distribution obtained from the calculated resolution function of the analyzing system. Deviations from this expected shape were attributed to the nonsubtractable background.

The polarization results are shown in Table I and

TABLE I. Neutron polarization distributions from the $C^{12}(He^3,n)O^{14}$ (g.s.) reaction.

E (MeV)	θ_1 (lab) (deg)	θ_2 (lab) (deg)	ϵ_0	$P_1\pm\Delta P_1$	E (MeV)	θ_1 (lab) (deg)	θ_2 (lab) (deg)	ϵ_0	$P_1\pm\Delta P_1$
2.24	20	70	−0.12	−0.14±0.06	2.39	20	80	−0.17	−0.21±0.03
	30	70	−0.07	−0.08±0.06		30	80	−0.27	−0.34±0.06
	40	70	−0.35	−0.41±0.09		40	80	−0.42	−0.53±0.07
	50	70	−0.50	−0.60±0.08		50	80	−0.68	−0.87±0.11
	60	70	−0.60	−0.77±0.12		60	80	−0.57	−0.78±0.09
	70	60	−0.69	−0.76±0.16		70	70	−0.47	−0.55±0.08
	80	60	−0.39	−0.45±0.12		80	70	−0.33	−0.42±0.10
						100	60	−0.14	−0.15±0.09
2.59	10	100	−0.10	−0.15±0.05	2.75	10	90	−0.06	−0.08±0.05
	20	90	−0.24	−0.33±0.06		20	90	−0.15	−0.21±0.05
	30	90	−0.35	−0.49±0.08		30	90	−0.20	−0.28±0.08
	40	90	−0.41	−0.57±0.09		40	90	−0.10	−0.14±0.06
	50	90	−0.08	−0.12±0.09		60	90	+0.17	+0.23±0.05
	60	80	0.00	0.00±0.05		80	80	+0.12	+0.15±0.06
	80	80	+0.07	+0.09±0.04		100	70	+0.19	+0.22±0.08
	100	70	+0.18	+0.22±0.05		120	70	+0.10	+0.12±0.06
	120	70	+0.10	+0.14±0.09					
2.93	10	110	−0.02	−0.04±0.05	3.10	10	100	−0.04	−0.05±0.06
	20	110	−0.18	−0.27±0.08		20	100	−0.05	−0.06±0.06
	30	100	−0.13	−0.18±0.05		40	100	+0.16	+0.22±0.06
	40	100	−0.06	−0.09±0.07		50	100	+0.32	+0.44±0.06
	60	100	+0.08	+0.12±0.05		60	100	+0.30	+0.42±0.06
	80	100	+0.18	+0.28±0.05		70	90	+0.22	+0.32±0.07
	100	80	+0.27	+0.34±0.04		80	90	+0.25	+0.35±0.09
	120	80	+0.32	+0.41±0.06		90	90	+0.15	+0.21±0.05
	140	70	+0.31	+0.36±0.05		100	90	+0.11	+0.16±0.06
						120	80	−0.03	−0.04±0.12
						140	80	−0.02	−0.03±0.16
3.30	20	110	+0.14	+0.18±0.06	3.49	10	110	+0.09	+0.12±0.07
	30	110	+0.30	+0.41±0.07		20	110	+0.25	+0.32±0.05
	40	110	+0.34	+0.48±0.09		40	110	+0.51	+0.68±0.07
	60	100	+0.34	+0.48±0.08		60	110	+0.21	+0.30±0.07
	70	100	+0.27	+0.37±0.07		80	100	−0.01	−0.01±0.05
	80	100	+0.09	+0.13±0.09		100	90	−0.06	−0.08±0.07
	100	90	−0.02	−0.02±0.11		120	90	−0.15	−0.21±0.17
	120	90	−0.07	−0.10±0.22					
3.70	20	110	+0.37	+0.47±0.07					
	40	110	+0.55	+0.72±0.08					
	60	110	0.00	0.00±0.07					
	80	100	−0.16	−0.22±0.08					
	100	100	−0.20	−0.28±0.18					
	120	100	−0.13	−0.19±0.15					

[25] W. D. Andress, Jr., F. O. Purser, J. R. Sawers, Jr., and R. L. Walter, Nucl. Phys. **70**, 313 (1965).

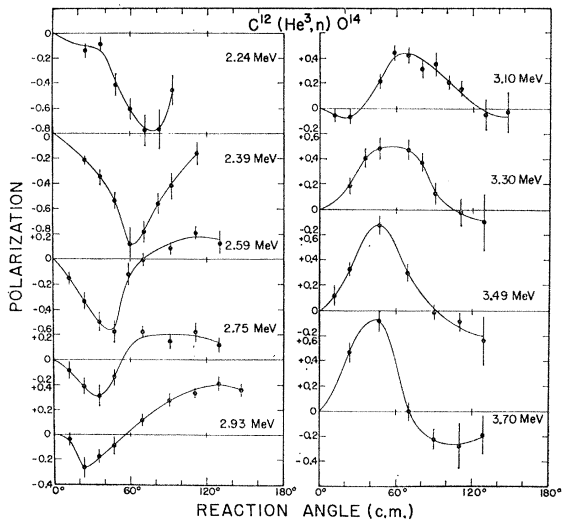

FIG. 3. Polarization distributions for the energies indicated as a function of c.m. angle. The curves are smooth lines drawn through the data points. The error bars indicate the estimated uncertainties as discussed in the text.

Fig. 3. Table I contains the mean incident He^3 energy in the laboratory system E, the laboratory angles θ_1 and θ_2, the background-corrected asymmetry ϵ_0, and the neutron polarization P_1. The listed uncertainty ΔP_1 includes the following errors: statistical uncertainty in the asymmetry, uncertainty in the average analyzing power P_2, and a liberal error estimate of 50% assigned to the magnitudes of both the room background and the nonsubtractable background. In Fig. 3, P_1 is plotted against the center-of-mass (c.m.) reaction angle θ_1 for the nine He^3 bombarding energies. The curves shown are smooth lines drawn through the data points. Large negative polarizations (up to -0.87) were found at the lower He^3 energies and high positive polarizations (up to $+0.72$) at the higher bombarding energies.

A pronounced change in the shape of the polarization distributions takes place around 3 MeV. This fact is illustrated in the lower part of Fig. 4, where a contour plot of the polarization data is presented. The nearly vertical contour lines at 3 MeV gradually become horizontal as the energy is increased, suggesting that above 3 MeV the direct mechanism is coming into predominance. Probably the strongest evidence that a change in reaction mechanism is occurring near 3 MeV is furnished by the excitation functions shown in the upper part of Fig. 4. Here Din's 0° and 90° excitation curves[8] are presented for the same energy range as the polarization contour plot. Below 3 MeV, two pronounced resonances appear in the 0° curve, and the 90° yield is in magnitude comparable to that at 0°. Above 3 MeV no more resonances are seen and the 0° peaking becomes pronounced as would be expected when an $l=0$ double-stripping reaction becomes predominant. (Since the contour plot was extracted from data obtained with targets that averaged 170 keV in thickness over the resonance region, the contour lines do not necessarily exhibit all of the detailed structure which may exist below 3.2 MeV.) Figure 5 shows the angular distributions of the differential cross section as measured by Din *et al.*[8] with a long counter and by Hollandsworth *et al.*,[9] using time-of-flight techniques. Below 3 MeV, the distributions tend to be either symmetrical or backward peaked; above 3 MeV, forward peaking is exhibited, especially in the case of Hollandsworth's data.

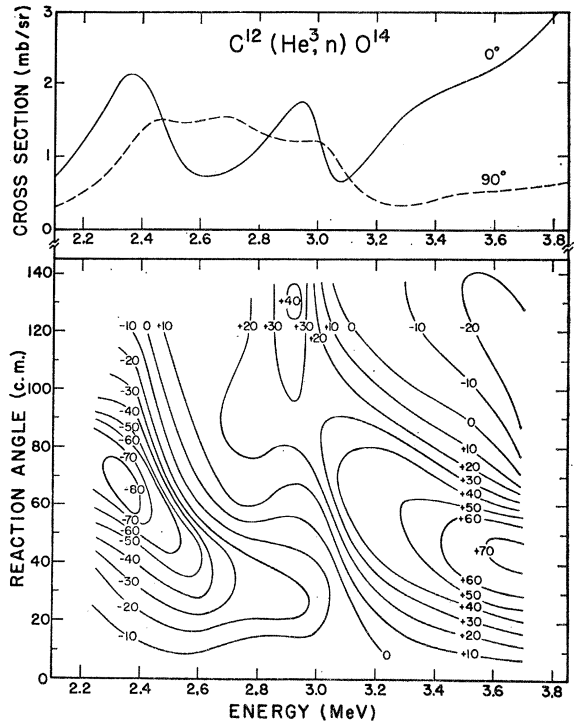

FIG. 4. Contour plot of the present neutron polarization data. The upper portion shows the 0° and 90° excitation functions by Din *et al.* (Ref. 8).

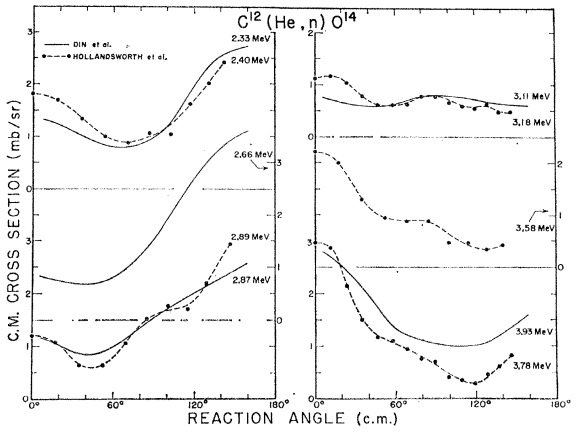

FIG. 5. C.m. angular distributions of the differential cross section. The solid lines are smooth lines drawn through the data points of Din *et al.* The dashed lines indicate the trend of Hollandsworth's data.

In order to determine to what extent the higher energy data can be represented by an $l=0$ double-stripping mechanism, a distorted-wave analysis was carried out for the 3.7 MeV angular distributions. This analysis is presented in Sec. IV.

III. He^3 ELASTIC SCATTERING

Three angular distributions of He^3 particles scattered elastically from C^{12} have been measured at 3.60, 3.70, and 3.80 MeV using a 70-keV-thick self-supporting carbon target. In addition, excitation functions with a 60-keV target have been taken at laboratory angles of 55°, 90°, and 125° in 25-keV steps from 3.50 to 3.91 MeV. Former elastic-scattering angular distributions have all been measured at energies greater than 4 MeV,[26–28] and only a few yield curves by Schapira *et al.*,[26] at laboratory angles of 15° and 125°, and by Kuan *et al.*,[29] at c.m. angles of 90°, 122.3°, and 164.5° are available in the energy range between 3.5 and 3.9 MeV.

The experimental arrangement was similar to the one described by Gerke *et al.*[17] In particular, the same scattering chamber was used. Silicon surface-barrier detectors of thickness 500 μ and 1000 μ were employed. The incident He^3 beam was monitored with a calibrated current integrator. The carbon target was mounted at 45° with respect to the incident-beam axis. Its thickness was determined by assuming pure Rutherford scattering for angles below 35° at the three energies at which angular distributions were taken. In addition, a 1200-keV-H_2^+ beam was used, giving a breakup proton energy of 600 keV. At this energy, the scattering at forward angles should be pure Rutherford scattering. The target thickness, extracted from measurements at 6 angles below 70°, was within 5% of the thickness obtained from the data at higher energies with the He^3 beam. In Sec. IV it is mentioned that the optical-model analysis of the 3.7-MeV elastic-scattering angular distribution suggests a 10% correction of the measured target thickness in order to obtain a better fit. Such a correction lies within the accuracy of our target-thickness determination and was therefore applied to the data.

The background was mainly caused by the different proton groups from the $C^{12}(He^3,p_i)N^{14}$ reactions, especially by the contributions from p_5 and p_6. This contaminant increased to 10% the uncertainty of the number of counts in the elastic-scattering peak at backward angles. At these angles, the magnitude of the correction had to be extrapolated using the $C^{12}(He^3,p_i)N^{14}$ data

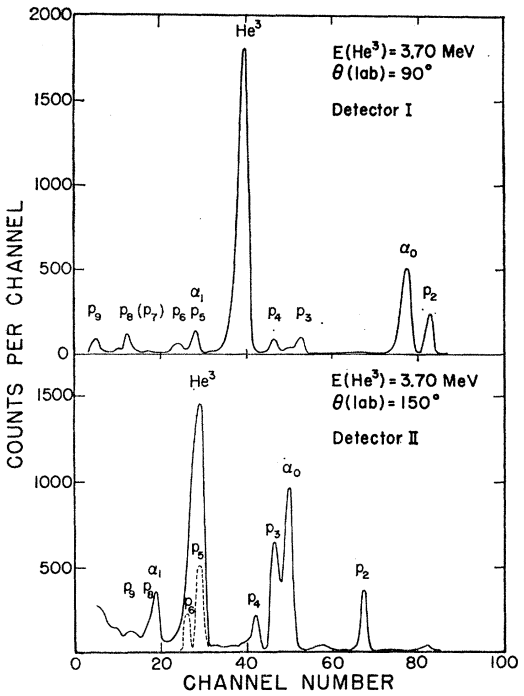

FIG. 6. Two sample spectra recorded with thick surface-barrier detectors. The upper part shows a well resolved He^3 elastic peak. This spectrum is characteristic for angles below 100°. The lower part shows the worst case; i.e., the He^3 peak at 150°.

of Kuan *et al.*[29] At angles below 100°, the elastic peak was dominant. At all angles, α groups from the $C^{12}(He^3,\alpha_i)C^{11}$ reactions were sufficiently well separated from the elastic peak. Figure 6 shows two sample pulse-height spectra for the 3.70-MeV angular distribution taken at laboratory angles of 90° and 150°. The separation of the various charged-particle groups from the elastic peak is obviously good at 90° and is relatively poor at 150°. The different groups were identified by using the elastic peak as an energy-calibration point. Channel zero corresponds to an energy of about 1 MeV.

The three angular-distribution measurements, taken by simultaneously using two detectors, covered the laboratory angular range of 20°–160° in 5° steps. They are shown in Fig. 7. The c.m. scattering angle is shown as the abscissa, and the ratio of experimental to Rutherford scattering is plotted as the ordinate. All three distributions exhibit similar shapes and magnitudes. Statistical errors were generally below 2%. The total relative uncertainties were estimated to be about 4% at forward angles and about 7% at back angles.

For the measurement of the excitation functions, the two detectors used for the angular distributions were placed at laboratory angles of 55° and 125°, and a third detector was positioned at 90°. The three yield curves are graphically represented in Fig. 8. The uncertainties are of the same size as mentioned above. As before, the ratio of experimental to Rutherford cross section is shown. In accordance with the data of Shapira *et al.*,[26]

[26] J. P. Schapira, J. O. Newton, R. S. Blake, and D. J. Jacobs, Nucl. Phys. **80**, 565 (1966).
[27] G. Parry, H. D. Scott, and S. Swierszczewski, Proc. Phys. Soc. (London) **77**, 230 (1961).
[28] J. J. Schwartz, W. P. Alford, L. M. Blau, and D. Cline, Nucl. Phys. **88**, 539 (1966).
[29] Hsin-Min Kuan, T. W. Bonner, and J. R. Risser, Nucl. Phys. **51**, 481 (1964).

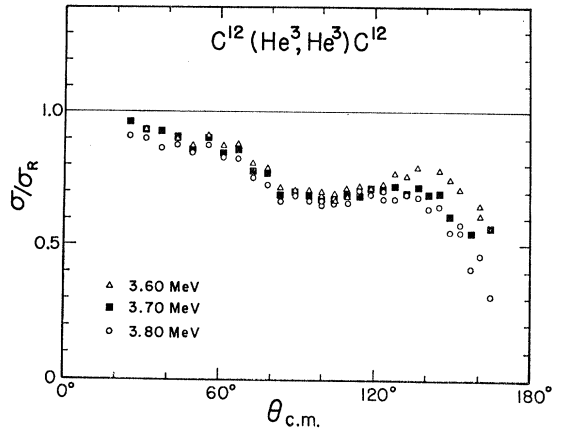

FIG. 7. Elastic-scattering angular distributions in the c.m. system for the three energies indicated. The ratio of experimental to Rutherford cross section is plotted.

and of Kuan *et al.*,[29] the experimental cross sections are smaller than the corresponding Rutherford cross sections throughout the energy range investigated, and the variation with energy is small and monotonic. Unlike the other nearby energy regions,[26,28,29] no resonance structure is exhibited. Thus, the optical model may perhaps apply to the elastic scattering of He^3 from C^{12} around 3.7 MeV.

IV. DISTORTED-WAVE ANALYSIS

A. Optical-Model Parameters

Optical-model parameters for the entrance channel of the $C^{12}(He^3,n)O^{14}$ (g.s.) reaction have been obtained from an analysis of the $C^{12}(He^3,He^3)$ elastic-scattering data at an energy of 3.70 MeV. This energy corresponds to the highest energy at which polarization distributions were measured. As was pointed out in Sec. II, the $C^{12}(He^3,n)$ reaction appears more likely to proceed via a double-stripping process at this energy than at the lower energies where polarization measurements were also taken. Thus the distorted-wave analysis has been restricted to the 3.70-MeV data.

The elastic-scattering computations were performed using the automatic search code HUNTER.[30] Four- and six-parameter searches were employed. For the four-parameter search, the optical-model potential $U(r)$ had the following form:

$$U(r)=V_c(r)-(V+iW)f(r,r_0,a),$$

where $V_c(r)$ is the Coulomb potential with Coulomb radius $R_c=r_cA^{1/3}$ fm, the quantities V and W are the real and imaginary potential-well depth parameters, and $f(r,r_0,a)$ is the Woods-Saxon form factor. For the six-parameter search, the form factor of the imaginary well uses radius and diffuseness parameters r_0' and a' which are independent of the corresponding parameters r_0 and a of the real well. The search routine was biased in favor of a real well potential of approximately three times the single nucleon potential. No such bias was introduced into the four-parameter search program. Finally, a spin-orbit potential of the Thomas type of fixed strength $V_s=6$ MeV and with form factor $(d/dr)f(r,r_0,a)$ was added to the optical potential and the six central-potential parameters were searched on again. All three searches lead to reasonably low χ^2 values. Table II lists the optical-model parameters and the χ^2 values obtained from the three search runs. The three parameter sets are labeled X, Y, and Z, respectively. The quantity χ^2 is defined by the equation

$$\chi^2=\frac{1}{N}\sum_{i=1}^{N}\left[\frac{\sigma_{\rm exp}(\theta_i)-\sigma_{\rm calc}(\theta_i)}{\Delta\sigma(\theta_i)}\right]^2,$$

where N, the number of data points, is 28, and $\Delta\sigma(\theta)$ is

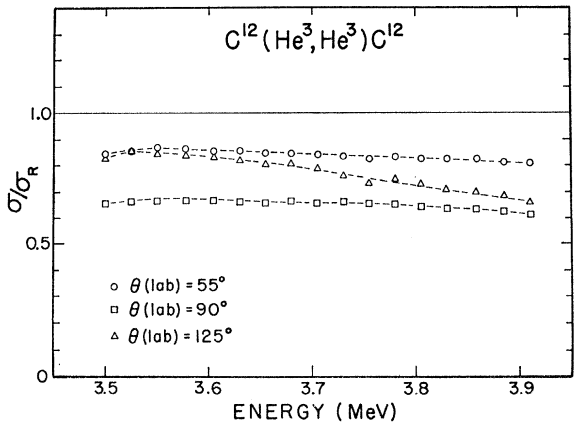

FIG. 8. Elastic-scattering excitation functions for laboratory angles of 55°, 90°, and 125°, respectively. The ordinate is the ratio of experimental to Rutherford cross section. The dashed lines indicate the trend of the data points.

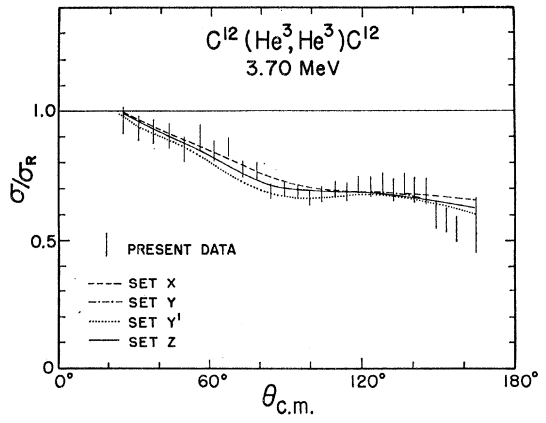

FIG. 9. Optical-model analysis of the 3.7-MeV elastic-scattering distribution. The experimental cross sections, indicated by their error bars, are plotted in units of the Rutherford cross section. The different fits are described in the text. The calculated curve obtained with set Y is almost identical to the one obtained with set Z with the exception of the angular region around 130°.

[30] R. M. Drisko (unpublished).

TABLE II. Optical-model parameters.

Reaction	Set	V (MeV)	r_0 (fm)	r_c (fm)	a (fm)	W (MeV)	W_D (MeV)	r_0' (fm)	a' (fm)	V_s (MeV)	χ^2
$C^{12}+He^3$	X	189.6	1.11	1.40	0.57	47.4	···	1.11	0.57	(6)	1.10
	Y	149.7	1.29	1.40	0.62	14.9	···	2.04	0.20	···	0.84
	Y′	150.0	1.25	1.40	0.65	15.0	···	1.93	0.47	(6)	1.32
	Z	150.5	1.28	1.40	0.62	15.0	···	2.03	0.22	6	0.85
$O^{14}+n$	A	44.0	1.25	1.25	0.65	···	1–5[a]	1.25	0.47–0.65[a]	4–12	
	B	43.5	1.29	1.25	0.73	···	2.9	1.26	0.53	4–12	

[a] The exact values used in the different DWBA calculations are noted in the text.

the error attached to the data which has been discussed previously. The inclusion of a spin-orbit potential of strength 6 MeV has very little effect on both the parameters and the elastic cross section. Also listed is a fourth parameter set with a somewhat higher χ^2 value, obtained from the output of the six-parameter search program. This set, called Y′, differs from set Y mainly in the parameters of the imaginary well. Figure 9 shows the theoretical curves in comparison with the measured elastic-scattering angular distribution. Here the ratio of experimental cross section to Rutherford cross section is plotted. The data points are represented with their estimated relative errors. After addition of a spin-orbit potential of strength 6 MeV to sets X and Y′, these two sets and set Z were subsequently used as parameters for the entrance channel of the $C^{12}(He^3,n)$ reaction.

Concerning the exit channel, a large uncertainty exists in the choice of the neutron parameters. Obviously an experimental measurement of elastic neutron scattering from the radioactive residual nucleus O^{14} is not possible. Elastic proton scattering from the mirror reaction $C^{14}(p,p)$ would furnish the next best set of parameters, but no optical-model analysis in the energy range of interest has yet been reported. Thus the neutron parameters were obtained through an averaging process over neutron and proton elastic-scattering data on light target nuclei.[12–17] The proton parameters were treated equal to the neutron parameters with the exception of the symmetry and the Coulomb correction[31] in the real-well strength. The lower part of Table II lists the neutron parameters thus chosen, or the range within which some of the parameters were allowed to vary in order to obtain a better fit to the reaction data. Here the absorptive term is of the derivative Woods-Saxon type, i.e.,

$$+i4a'W_D(d/dr)f(r,r_0',a'),$$

where $f(r,r_0',a')$ is again the Woods-Saxon form factor. Set A is based on a more "standard" geometry.[14,15] Set B is essentially an average over all optical-model parameters obtained by Gerke *et al.*,[17] from an analysis of their $C^{13}(p,p)$ elastic-scattering data in the energy range 1.55–2.38 MeV.

[31] F. G. Perey, Phys. Rev. **131**, 745 (1963).

B. Reaction Analysis

Zero-range distorted-wave calculations for the $C^{12}(He^3,n)$ reaction at 3.70 MeV were made using a two-particle transfer option in the computer code JULIE.[32] In particular, the two captured protons were described by Woods-Saxon single-particle wave functions.[33] The well depth was adjusted to give an eigenstate with an energy of half the difference in binding energy of C^{12} and O^{14}. With a 12-term harmonic oscillator expansion, the form factor was accurately represented over the range in which it contributes to the DWBA integrand. A few calculations were also made using a slightly different kind of form factor[34] derived from oscillator single-particle functions, but with an exponential tail (Hankel function) smoothly matched on to the form factor. The resulting angular distributions did not differ significantly from those produced by the form factor with Woods-Saxon single-particle functions. The two protons were described by pure $(p_{1/2})^2$, $(p_{3/2})^2$, and $(f_{7/2})^2$ shell-model configurations as well as by different combinations of these three configurations.

Almost identical cross-section and polarization distributions were obtained for pure $(p_{1/2})^2$ and $(p_{3/2})^2$ wave functions. An $(f_{7/2})^2$ configuration gave different results, filling in the valley of the cross-section angular distribution and diluting the polarizations. However, no large contributions from $f_{7/2}$ wave functions are expected. Because of the uncertainty of the optical-model parameters in the exit channel, the expected predominance of a $(p_{1/2})^2$ configuration for the captured particles, and the similarity of the $(p_{1/2})^2$ and $(p_{3/2})^2$ calculation, the $(p_{1/2})^2$ wave function was employed throughout the fitting procedure.

Using the optical-model parameter set Y′ for the entrance channel, set A with a spin-orbit strength of 6 MeV, and an imaginary well diffuseness parameter of 0.47 fm for the exit channel, the $C^{12}(He^3,n)$ angular distribution can be reasonably well described with a neutron absorptive well depth W_D of 1.5–3.0 MeV. Figure 10 shows the effect of different values of W_D on the cross section and polarization distributions. The

[32] R. H. Bassel, R. M. Drisko, and G. R. Satchler, Oak Ridge National Laboratory Report No. ORNL-3240 (unpublished).
[33] R. M. Drisko and F. Rybicki, Phys. Rev. Letters **16**, 275 (1966), and references therein.
[34] N. K. Glendenning, Phys. Rev. **137**, B102 (1965).

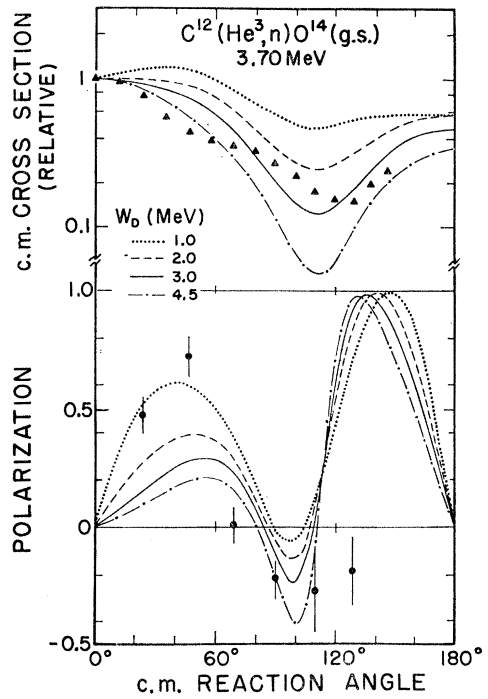

FIG. 10. Influence of the neutron absorptive well depth parameter W_D on the DWBA fits to the cross section and polarization distributions. The cross-section data, indicated by triangles, were interpolated from Hollandsworth's measurements at 3.58 and 3.78 MeV. The polarization data, indicated by solid circles with error bars, represent the present measurements at 3.70 MeV.

cross-section data shown in the following figures are those of Hollandsworth *et al.*,[9] interpolated from his measurements at 3.58 and 3.78 MeV. Unlike the elastic scattering fits, the stripping fits were normalized to the 0° cross section. This was necessary since it is too early in the development of the theory to be confident of normalizing the calculations, even for a transition in which one has confidence in the bound-state wave function of the states involved. The high polarizations measured at forward angles are best approximated with the lowest imaginary well depth W_D. On the other hand, the theoretical curve dips only slightly negative for a low W_D. All calculated curves exhibit very large positive polarizations at backward angles.

The influence of the neutron spin-orbit strength V_s is depicted in Fig. 11. Here set Z is used in the entrance channel, set A with $W_D=2.5$ MeV, $a'=0.65$ fm, and V_s is a variable parameter in the exit channel. A spin-orbit strength greater than 9 MeV causes the reaction cross section to fall off at high backward angles, while a V_s of 4 MeV raises the extreme backward cross section to almost its value at 0° and produces only small positive polarizations at forward angles. Thus, a neutron spin-orbit strength of about 6 MeV is suggested in accordance with Perey's[15] summary of (p,p) polarization data. Perey also favors the spin-orbit form factor parameters $r_s=1.12$ fm and $a_s=0.47$ fm. As can be seen in Fig. 11, Perey's parameters result in a slightly better fit to the polarization data without significantly changing the reaction cross section. The effect of changing the neutron absorptive diffuseness parameter a' from 0.47 to 0.65 fm is of minor importance. It is a striking fact that the He^3 spin-orbit strength has a very small influence on the theoretical curves. Even a variation of V_s from 0 to 20 MeV does not produce different shapes, at least as long as optical-model parameters are employed which give good fits to the He^3 elastic-scattering data. Hence, the neutron spin-orbit term is mainly responsible for polarization effects.

Finally, Fig. 12 shows DWBA fits for different sets of entrance- and exit-channel parameters. The He^3 sets X, Y′, and Z are used as input parameters together with the neutron set A with $W_D=2.5$ MeV, $V_s=6$ MeV, and $a'=0.65$ fm. In addition, set B, derived from Gerke's[17] proton parameters with $V_s=6$ MeV, is employed in the exit channel together with the He^3 sets X and Z. Apparently the polarization distributions at forward angles are better reproduced with Gerke's average-parameter set than with set A, which employs a more or less standard geometry. Also, the four-parameter set X approximates the forward-angle polarization data better than the seven-parameter set Z, which gives the best fit to the He^3 elastic-scattering distribution. On the other hand, the cross-section distributions, obtained from set X, exhibit for both neutron sets a shallow valley and would need an imaginary potential-well depth W_D in the exit channel of about 4 MeV in order to agree better with Hollandsworth's data.

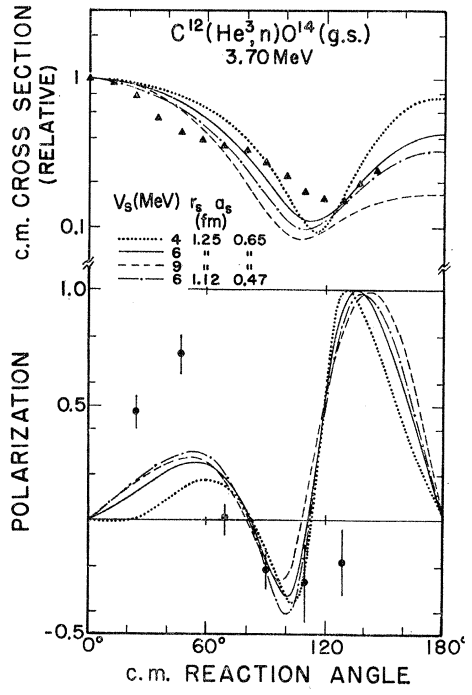

FIG. 11. Influence of the neutron spin-orbit strength V_s and its form-factor parameters r_s and a_s on the DWBA fits to the cross section and polarization distributions.

In conclusion, the zero-range distorted-wave method assuming an $l=0$ double-stripping mechanism and using "reasonable" optical-model parameters, succeeds in fitting the gross structure of the $C^{12}(He^3,n)$ reaction cross section although no detailed agreement was achieved. Reasonably good fits to the polarization data were obtained, but somewhat at the expense of the cross-section agreement.

V. DISCUSSION

Considering the fact that a light target and low incident energies were used, the results obtained from the DWBA calculations are encouraging from the standpoint of a direct-interaction mechanism. The He^3 elastic-scattering data could be fitted with both four- and six(seven)-parameter potentials, and the optical-model parameters extracted from these fits reproduced the reaction angular distribution reasonably well. Also, deviations from the best-fit He^3 elastic-scattering parameters generally resulted in worse fits for the reaction distribution. More proton and neutron elastic-scattering data for low energies and light targets are needed in order to obtain reliable optical-model parameters for the exit channel. However, an optical-model analysis of such measurements is complicated by the presence of, and the interference with, compound nucleus resonances.

Our polarization calculations imply that the neutron spin-orbit strength rather than the He^3 spin-orbit strength is responsible for polarization effects. The calculations do reproduce the positive sign at forward angles and the negative sign near the cross-section minimum. Since the $C^{12}(He^3,n)$ data indicate strong compound nucleus effects below 3 MeV, such effects could still be pronounced at 3.7 MeV, especially in an angular region where the stripping amplitude is small. Thus compound nucleus contributions may well account for the failure to give detailed agreement with the cross-section measurements and to closely reproduce the polarization angular distributions. It would be interesting to obtain more polarization data at larger backward angles and in higher energy regions to see whether the large positive backward peaking exhibited in all theoretical curves has an experimental counterpart.

Our $C^{12}(He^3,n)$ polarization measurements are evidence that present techniques are sufficiently advanced to perform double-scattering experiments with neutron-reaction cross sections of less than 1 mb. With incident He^3 beam intensities of 6 μA and a target thickness of 200 keV, the accelerator time required to measure one polarization angular distribution with reasonable accuracy is of the order of one day. Recently, a second (He^3,n) polarization experiment using a Be^9 target has been performed in this laboratory.[35] In order to obtain additional information about the importance of double-stripping processes, more polarization measurements of neutrons from He^3-induced reactions are desirable.

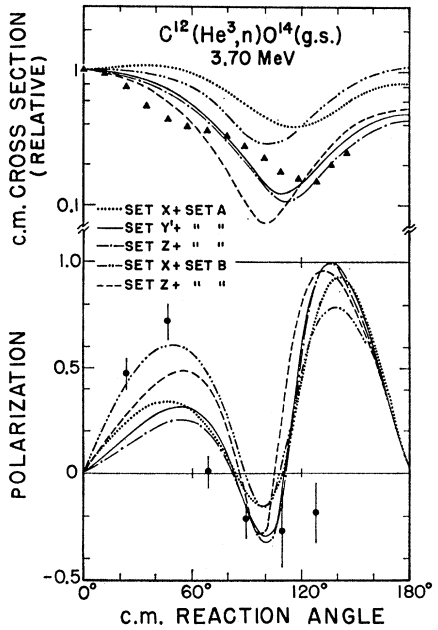

FIG. 12. DWBA fits to the cross-section and polarization distributions using the "best fit" He^3 elastic-scattering parameters in the entrance channel and two different neutron sets A and B in the exit channel.

ACKNOWLEDGMENTS

We would like to thank Dr. D. R. Tilley for the use of the scattering chamber and H. R. Weller for his help in setting up the elastic-scattering experiment. We would also like to acknowledge the assistance of G. L. Morgan in accumulating the polarization data and of Mrs. M. Bailey in drawing the figures. Finally we wish to thank Dr. C. E. Hollandsworth for permission to use his cross-section data prior to publication. The authors from Duke University wish to thank the staff of the Electronuclear Laboratory at Oak Ridge for their hospitality during the time the DWBA calculations were performed.

[35] R. S. Thomason, L. A. Schaller, and R. L. Walter, Bull. Am. Phys. Soc. **12**, 88 (1967).